UNIFIED FRAMEWORK FOR ANALYSIS AND DESIGN OPTIMIZATION OF A MULTIROTOR UNMANNED AERIAL VEHICLE

Daejin Lim[1], Hyeongseok Kim[1], Bosung Lee[2], Kwanjung Yee[3]

[1]Dept. of Mechanical and Aerospace Engineering
Seoul National University, Seoul, Republic of Korea
djlim8433@snu.ac.kr / khs931113@snu.ac.kr

[2]Unmanned Vehicle Advanced Research Center,
Korea Aerospace Research Institute, Daejeon, Republic of Korea
gotocloud@kari.re.kr

[3]Institute of Advanced Aerospace Technology,
Seoul National University, Seoul, Republic of Korea
kjyee@snu.ac.kr

Abstract

Designing a small-scale multirotor UAV is a complicated procedure that requires multi-disciplinary analyses including rotor aerodynamics, structure, and electric propulsion system. However, owing to the complexity of multi-disciplinary analyses, the design of conventional multirotor UAVs heavily relies on the empirical methods through experimental data or legacy selections. These methods not only lack the firm physical basis for selecting the component, but also are extremely time-inefficient, requiring numerously repetitive experiments. In order to establish a systematic design procedure for multirotor UAVs, the unified design optimization framework, titled as Conceptual Layout Optimization for Universal Drone Systems (CLOUDS), was developed in this study. CLOUDS consists of five multi-disciplinary analysis modules including aerodynamics and electric propulsion system. Utilizing these modules, it can accurately estimate the performance of the system in response to the variation of the combination of components, showing high accuracy of predicting the flight time within 10% deviation. As such, the optimal configuration of multirotors could be designed for a specific mission. Based on the developed framework, correlations between the variables are found using Self-Organizing Maps (SOM) and Analysis of Variance (ANOVA). Additionally, design optimizations were conducted for two hover missions with different time as an example. The optimum design solution was presented by analyzing the optimization results.

NOMENCLATURE

A_{max}	Maximum allowable current of ESC
B	Tip loss factor
c_{max}	Maximum chord length of a rotor blade
c_{root}	Root chord length of a rotor blade
c_{tip}	Tip chord length of a rotor blade
C_d	Drag coefficient
C_T	Thrust coefficient
C_P	Power coefficient
CG_R	Length to center of gravity position
dC_T	Incremental thrust coefficient
dC_{p_i}	Incremental induced power coefficient
dC_{p_0}	Incremental profile power coefficient
d_{rod}	Inner diameter of a support rod
D	Drag force on vehicle
$D_{landing}$	Outer diameter of a landing gear
D_{rod}	Outer diameter of a support bar
D_{rotor}	Diameter of a rotor
D_t	Throttle command
η_m	Efficiency of a motor
g_f	Acceleration factor
I_0	No-load current
I_a	Avionics current

I_d	Drive current
I_m	Motor current
$I_{m_{avg}}$	Averaged motor current
I_p	Payload current
I_t	Total current
I_{zz}	Second moment of area
κ	Induced power factor
K_t	Motor torque constant
K_v	Motor speed constant
λ	Inflow ratio
λ_c	Inflow ratio by climbing speed
l_{tip}	Tip clearance between rotors
L	Length of a support rod
$L_{landing}$	Length of a landing gear
n_{safe}	Safety factor
N_{rotor}	The number of rotors
P_{elec}	Electric power
P_{mech}	Mechanical power
P_{max}	Maximum continuous electric power
P_{Co}	Copper loss
P_{Ir}	Iron loss
P_{Me}	Mechanical loss
P_{St}	Stray loss

$r_{c_{max}}$	Position to maximum chord
r_{root}	Position to root cut
$r_{\theta_{max}}$	Position to maximum twist angle
R_b	Total inner resistance in a battery
R_{cell}	Inner resistance in 1 cell battery
R_{center}	Centre plate radius
R_{esc}	Inner resistance of ESC
R_m	Inner resistance of motor
R_{rotor}	Radius of a rotor
RPM	Revolutions per minute
σ	Solidity of a rotor
σ_{allow}	Allowable stress
σ_{max}	Maximum stress
σ_{ult}	Ultimate stress
θ_{max}	Maximum twist angle
θ_{pitch}	Vehicle pitch angle
θ_{root}	Twist angle at root of blade
θ_{tip}	Twist angle at tip of blade
T_{req}	Required thrust
V_b	Total battery voltage
V_{emf}	Motor back EMF voltage
V_F	Flight speed
V_m	Motor voltage
$V_{m_{avg}}$	Averaged motor voltage
W_{esc}	ESC weight
W_m	Motor weight
W_{total}	Total vehicle weight

1. INTRODUCTION

Since the advent of the multirotor type Unmanned Aerial Vehicles (UAVs) that use multiple rotors, the application area has been enlarged due to their advantages like maneuverability, controllability, and manufacturability. Especially, the small size and hovering capability make multirotor extensively utilized in not only the industry fields but also the commercial markets such as leisure and filming[1,2]. Various configurations of the multirotors have recently been developed and commercialized in light of popularization and the increased reliability of an Electric Propulsion System (EPS). The EPS is commonly equipped to the multirotors because it has superior characteristics such as low weight, low noise, and high efficiency to the engine system. In the EPS, an electric motor and a rotor combined, constitute a driving unit that provides thrust for the multirotors. The thrust generated by the rotor is conventionally controlled by varying the RPM of the motor. This control method establishes the driving part where aerodynamics and electrical system are tightly coupled, ultimately instigating a substantial difference in the performance according to the combination of rotors, motors, and batteries. Therefore, it requires conducting multi-disciplinary analysis considering the rotor aerodynamics and the EPS to design and analyze the multirotors.

Despite its importance, conventional multirotors are designed mainly based on the empirical methods through experimental data or legacy selections due to the complexity of the aforementioned multi-disciplinary analysis. These methods not only lack the solid physical basis for selecting components but also are highly time-inefficient, requiring numerously repetitive experiments. In addition, these methods are incapable of considering a specific mission or a flight environment where the UAV actually flies. In order to overcome these limitations, numerous studies[3-5] have been carried out on designing multirotors. Bershadsky[3] developed a sizing tool for multirotors named as Electric Multirotor Sizing Tool (EMST). The authors present the weight estimation method using the representative parameters of components in a multirotor. Despite its contribution, the presented tool uses constant motor efficiency value that is incapable of estimating the efficiency of a motor that changes by a combination of a motor and a rotor. Winslow[4] documents a sizing process based on estimating the weight and analyzing the aerodynamics of a rotor. This method predicts the total weight of a vehicle within 4% deviation. However, it lacks the analysis for EPS, so that performance analysis is not conducted. Gur[5] carries out multi-disciplinary optimizations for UAV climbing and loitering, and performs sensitivity analysis. The authors also present the modeling method for motors. Other tools for predicting flight time of UAVs exist as well as those above. The eCalc+), one of the tools, provides the performance with the consideration of the motor efficiency calculated by users selecting off-the-shelf components. This tool is intended to calculate the performance of the multi-rotors, and uses simple equations in aerodynamics resulting in relatively less rigorous results. Moreover, it handles only hover flight, not a specific mission.

In summary, the existing methods and tools are incapable of estimating the flight performance because of not accounting for EPS, or their analysis accuracy is limited since they do not reflect the inherent characteristic of the EPS. Furthermore, no study has been conducted to design an optimum configuration for a specific mission considering the body frame structure. As such, it is necessary to establish a systematic design procedure for a multirotor in consideration of the inherent characteristic of the EPS and the frame structure.

To this end, a unified framework for analysis and design optimization of multirotors has been developed in this study. This optimization framework, titled as Conceptual Layout Optimization for Universal Drone Systems (CLOUDS), is able to suggest an optimum combination of the components of multirotors for a specific mission profile. In addition to the developed tool, a novel analysis process of the EPS and modeling methods are presented to increase the accuracy and efficiency of the calculation.

+) eCalc xcopter, http://www.ecalc.ch/xcoptercalc.php

This paper describes the development of the framework with a detailed explanation of the design procedure, features, and the structure of CLOUDS. Afterward, details of modeling methods by each disciplinary and the analysis process of the EPS are proposed. The proposed methods are verified in each analysis module, followed by the validation for whole UAV system through comparison with flight test results. The correlations between the variables and sensitivity on performance are found using the SOM and ANOVA. Finally, the design optimizations are conducted for specific objectives with the framework.

2. THE STRUCTURE OF CLOUDS

The developed framework, CLOUDS, consists of dual modes - analysis and design, so that it is capable of analyzing the flight performance of the multirotors and deriving an optimal design. In analysis mode, with users specifying specifications of each component and a mission, CLOUDS provides useful data including flight time after checking the feasibility of the vehicle. Within the calculation, multi-disciplinary analysis algorithm is used which is comprised of five disciplinary modules: Estimation, Attitude, Structure, Aerodynamics, and EPS. Based on this analyzer, the design mode suggests a suitable configuration for a given purpose at the conceptual design phase.

An overview of the design algorithm that has a hierarchical structure, mission segment analysis and module analysis (Figure 1), is described. Like conventional design methods for rotary wings, the optimization procedure starts with a specific mission profile. 1) Before the mission profile is divided into each segment, the Estimation module is first executed. This module estimates the weight of components: a rotor, a motor, a battery, an electric speed controller (ESC), and a body frame. The characteristic values of electrical parts and the layout of a vehicle are also obtained here using the design variables and parameters. 2) The multi-disciplinary analyzer calculates the performance of the vehicle in each separated mission segment. The Depth of Discharge (DoD) of the battery is obtained at the end of the segment analysis. This value is used as the initial value to calculate battery voltage in the EPS at the next segment. 3) When all segment analyses are carried out, the optimizer checks the feasibility of the vehicle based on several values like final DoD. If the multirotor is constructed with a feasible combination of components, the optimizer evaluates the fitness of the solution. 4) This process is iterated by changing design variables until satisfied termination criteria are met. The available optimization methods are as follows: Sequential Least Squares Programming (SLSQP)[6], Particle Swarm Optimization (PSO)[7], and Genetic Algorithm (GA)[8].

The analysis flow at a mission segment level is shown in Figure 2. Four analysis modules except the Estimation are executed sequentially. Utilizing the total vehicle weight W_{total} estimated from the Estimation module, the Attitude module calculates a pitch angle of the vehicle θ_{pitch} and the thrust T_{req} required at each rotor. The T_{req} is one of the input values for the Structure and the Aerodynamics module. The Structure module checks whether the support rod of the body frame can tolerate the load. In the Aerodynamics module, the RPM and the mechanical power P_{mech} of rotors are calculated at the given condition.

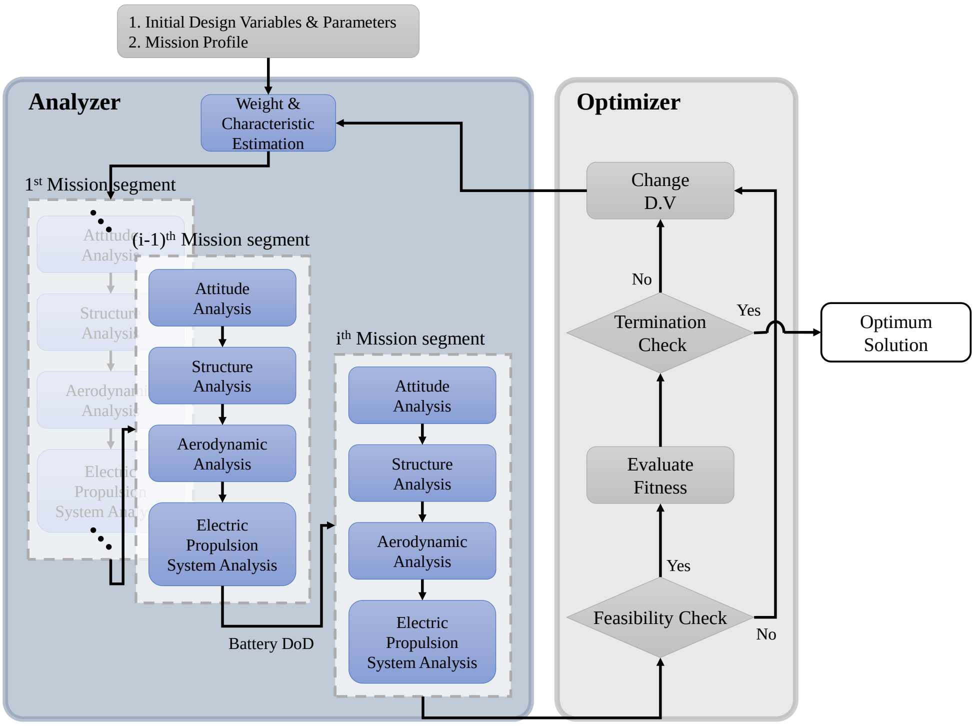

Figure 1: Overall Design process of CLOUDS

The EPS analysis module is executed at last. In this module, motor voltage V_m, motor current I_m, and motor efficiency η_m are calculated to drive the rotors at given RPM with the P_{mech}. The used battery capacity and DoD are also calculated. As mentioned previously, this DoD value is used in the next segment analysis or feasibility check by the optimizer.

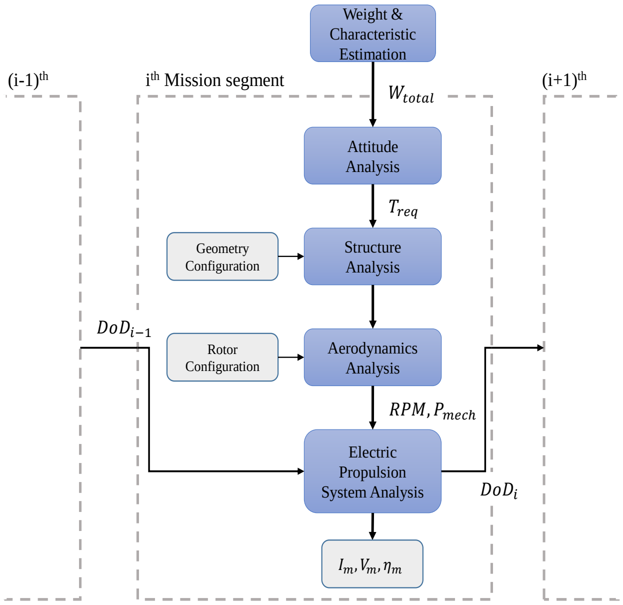

Figure 2: Analysis process of a mission segment

3. THE ANALYSIS MODULES OF CLOUDS

The following section documents the five modules constituting the multi-disciplinary analysis algorithm. The description is presented in a sequence of the Estimation, Attitude, Structure, Aerodynamics, and EPS module.

3.1. Estimation module with modeling

Although the multirotor UAVs consist of many components depending on its purpose, the general components include rotors, motors, batteries, ESCs, and a body frame. In this section, presented is the method for estimating the weight and characteristic values from key parameters as well as modeling method for each component. Some of the weight trends are from Ref. [3], and the others are empirically obtained as needed.

3.1.1. Rotor

Depending on the dimension of a multirotor, various size of the rotor is used from 2 to 50 inches. The weight of a rotor is dependent to its radius R_{rotor} and materials[3]. Even if rotors have the same radius and weight, the aerodynamic performance is significantly different according to the geometry of their blade. When calculating, it is the best to use exact geometric data, which is not always available.

Thus, the 10 configuration parameters are adopted to model a rotor blade. As shown in Figure 3, these parameters are related to chord length and twist angle, including R_{rotor}.

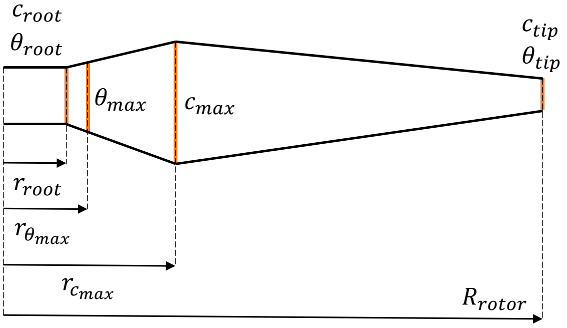

Figure 3: Configuration parameters of a rotor blade

It is assumed that the distribution of chord length and twist angle between the positions changes linearly. This linear blade model produces the aerodynamic performances close to those from exact geometrical data, showing small difference of about 3% at the same condition (Figure 4). The experimental data is obtained from static thrust test by Korean Aerospace Research Institute (KARI). This model allows analyzing the rotor performance only with minimal geometrical data available.

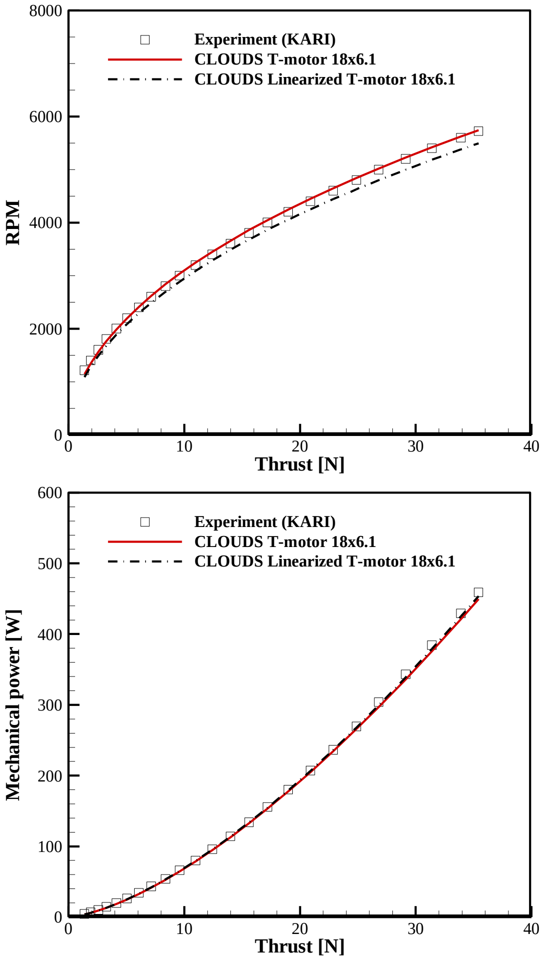

Figure 4: Validation of linearized rotor blade model

Presented at 44th European Rotorcraft Forum, Delft, The Netherlands, 19-20 September, 2018

3.1.2. Brushless DC motor (BLDC motor)

The BLDC motors are preferred for small-scale multirotors due to its advantages of higher efficiency and lower noise than brushed motor[3,5]. One of the critical parameters when selecting a motor is motor speed constant K_v. This value indicates how fast the motor would rotate with the voltage supplied in an unloaded condition. The K_v is highly related to the motor weight W_m and the characteristics of the motor such as the inner resistance R_m, no-load current I_0, and maximum continuous electric power P_{max}.

In this study, based on the data of commercialized motors for UAVs, the trends were found for the weight and the characteristics. First, as shown in Figure 5, the higher K_v motor has the lower W_m, similar to the results of Bershadsky[3] and Gur[5]. Eq. (1) gives the weight trend of the motor.

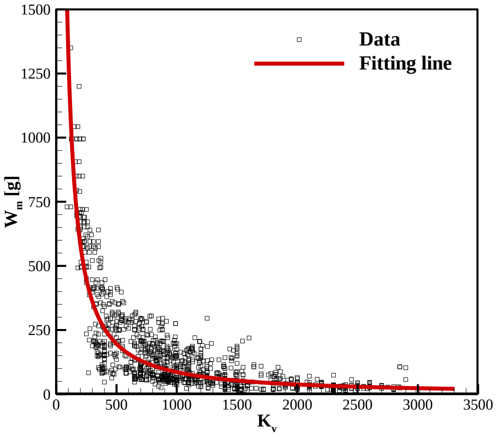

Figure 5: BLDC motor weight trend

(1) $$W_m = 323{,}392 K_v^{-1.192} \quad [\mathrm{g}]$$

The inner resistance of motor R_m relation with the K_v and the W_m is shown in Figure 6. As multiplication of $K_v W_m$ becomes large, the resistance gets small. The R_m is calculated by Eq. (2).

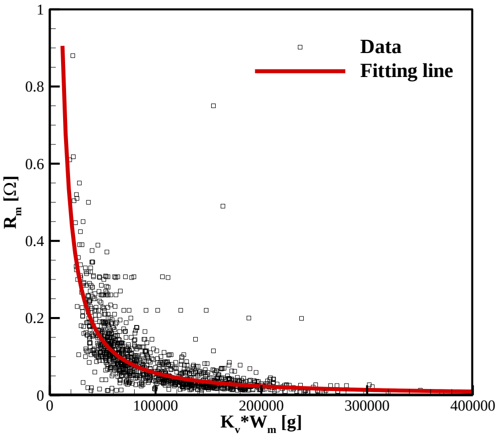

Figure 6: Inner resistance trend

(2) $$R_m = 181{,}867 (K_v W_m)^{-1.3} \quad [\Omega]$$

Figure 7 presents the relationship between the no-load current I_0 versus the R_m. The following trend is apparent; small resistance induces large no-load current.

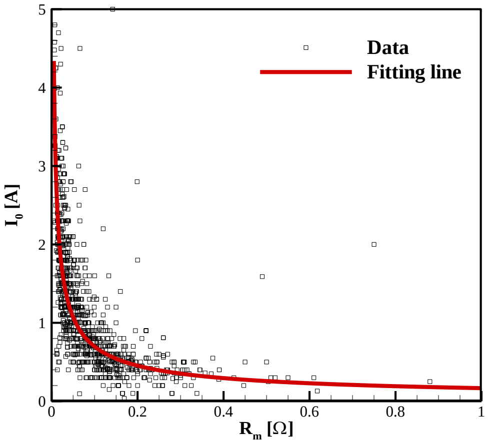

Figure 7: No-load current trend

(3) $$I_0 = 0.1667 R_m^{-0.622} \quad [\mathrm{A}]$$

In the present study, maximum continuous electric power P_{max} is considered additionally to make sure the motor would operate safely. The P_{max} is directly proportional to the W_m (Figure 8).

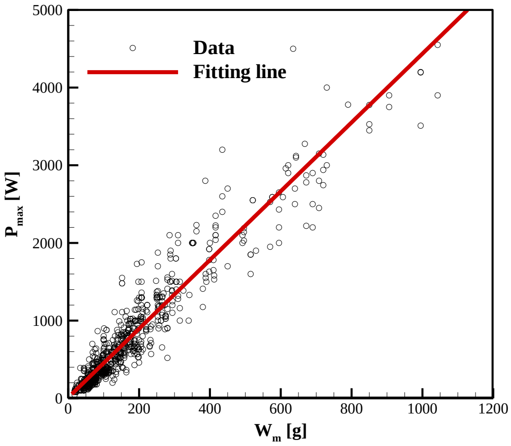

Figure 8: Maximum continuous electric power trend

(4) $$P_{max} = 4.4265 W_m + 9.8975 \quad [\mathrm{W}]$$

Through the relations presented above, the characteristic values could be estimated by using just one parameter or K_v. In the CLOUDS, the users can select the option whether they input real value or use trend estimation.

3.1.3. Lithium polymer battery (LiPo battery)

LiPo batteries are commonly used as a power source in UAVs because of their higher energy density than others like the gasoline system. The main parameters deciding the weight and performance of a LiPo battery are the number of cells, capacity, and allowable C-rate. The weight of a battery is dependent on total capacity and the number of cells[3]. Although LiPo cells are known nominally to have voltage of around 3.7 V per cell, the actual voltage per cell is 4.2 V when fully charged, and it drops depending on how much they are charged (DoD) and how fast they are used (C-rate). In the CLOUDS, the battery performance model is based on the data of discharge experiment+). The ambient temperature effect on the voltage drop phenomenon is also considered[9].

3.1.4. ESC

The ESCs coupled with the BLDC motors change the RPM of the motor to control the thrust and power generated at the motor by taking Pulse-Width Modulation (PWM) signal. When selecting the ESC, the maximum allowable current A_{max} of it is the critical parameter. This value must be higher than the motor current to prevent overheating and system failure. Figure 9 and Figure 10 show the trend of the ESC weight W_{esc} and the ESC resistance R_{esc} as the function of the A_{max} respectively. The equations are presented under each figure. The W_{esc} linearly goes up and the R_{esc} exponentially goes down as the A_{max} increases.

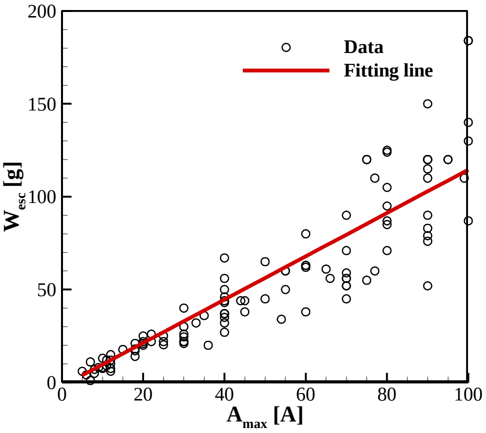

Figure 9: ESC weight trend

(5) $$W_{esc} = 1.1652A_{max} - 2 \quad [\mathrm{g}]$$

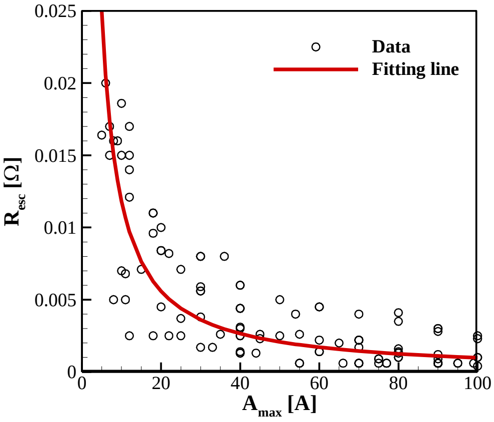

Figure 10: ESC resistance trend

(6) $$R_{esc} = 0.1423A_{max}^{-1.081} \quad [\Omega]$$

3.1.5. Body Frame

The body frame is the structure of a multirotor to support the components mentioned before, avionics like Flight Control Computer (FCC) and a payload. Present study assumes that the layout of the body frame has radial structure shown in Figure 11. The support rod and landing gear rod is a cylindrical tube shape, and the center body is a thin circular plate. The geometry is constructed using input parameters: rotor radius R_{rotor}, rod length L, rod diameter D_{rod}, and the number of rotors N_{rotor}.

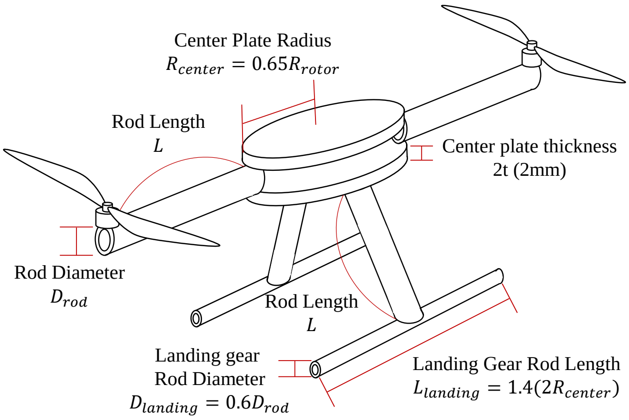

Figure 11: The layout assumption

Before estimating the weight of the body frame, the geometrical interference inspection is conducted in advance. Tip clearance l_{tip} is calculated by Eq. (7) deduced from the geometric relation shown in Figure 12.

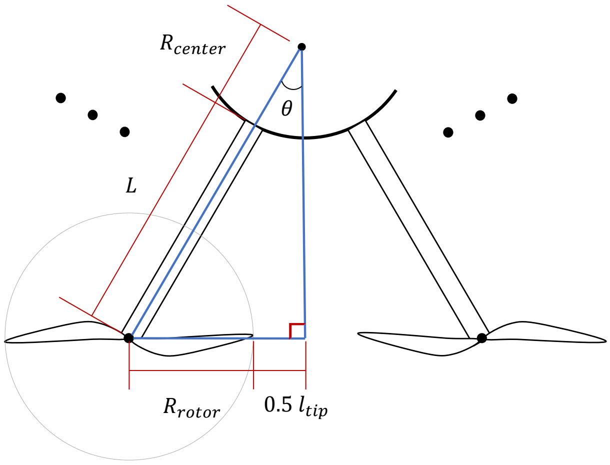

Figure 12: Geometric relation for rotor tip clearance

(7) $$sin(\theta) = \frac{R_{rotor}+0.5l_{tip}}{L+R_{center}} \quad , \ \theta = \pi/N_{rotor}$$

By rearranging the Eq. (7) with known values, the l_{tip} is obtained. In case of $l_{tip} > 0$, the body frame is constructed, and then, the weight of the frame is estimated summing up the weights of the rods, the center plates, and the landing gear.

+) https://www.rcgroups.com/forums/showthread.php?1579483-Does-cold-%28storage%29-affect-Lipo-and-Life-battery-longevity accessed at 17/07/2018

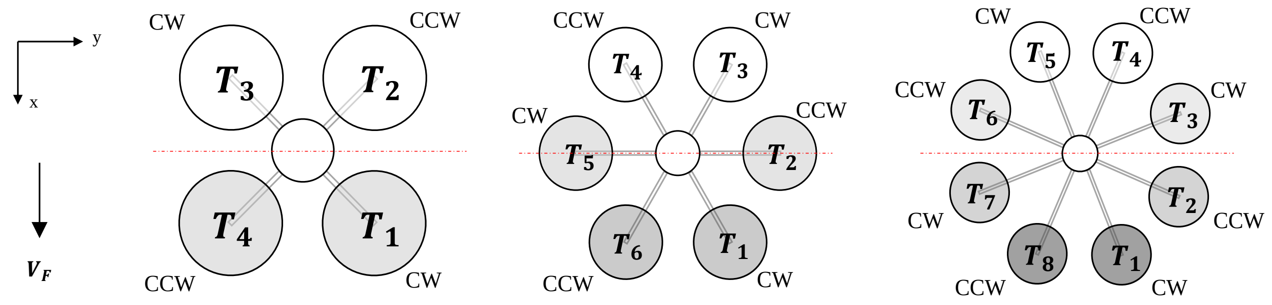

Figure 13: Schematics of multirotors in forward flight

3.2. Attitude analysis module

The Attitude module calculates the required thrust T_{req} and vehicle's pitch angle θ_{pitch} in a given flight condition. It is assumed that all flight status are steady state, and the vehicle flies level flight with X-position in the forward dash. For rolling mement equiliribrium, the paired rotors with x-axis symmetry generate the same thrust. In addition, adjacent rotors rotate in the opposite direction for yawing moment equilibrium (Figure 13). Therefore, under the condition that yawing and rolling moment equilibrium is established, the T_{req} and the θ_{pitch} can be obtained by satisfying only pitching moment equilibrium condition. It is assumed that the thrust variance required to generate θ_{pitch} occurs at the rotors located furthest from the center dashed line (Figure 13).

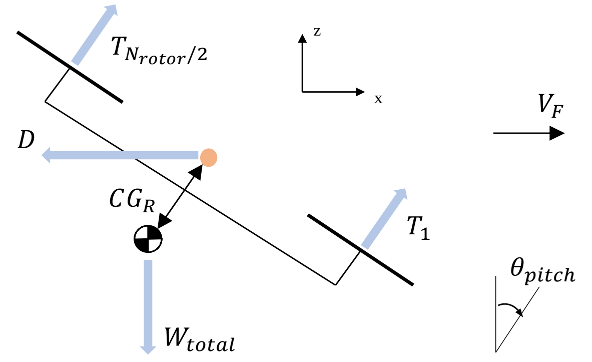

Figure 14: Forces in forward flight

Figure 14 shows the forces acting on the vehicle in forward flight. For a steady flight, the sum of forces and moment applied to the vehicle should be zero. The related equations are following.

(8) $$T_i = T_{N_{rotor}-i+1} \quad 1 \le i \le N_{rotor},\ i\!: integer$$

(9) $$\Sigma F_x = \left(\Sigma_{i=1}^{N_{rotor}} T_i\right) sin\theta - D = 0$$

(10) $$\Sigma F_z = \left(\Sigma_{i=1}^{N_{rotor}} T_i\right) cos\theta - W_{total} = 0$$

(11) $$\Sigma M_y = 2\left(T_{N_{rotor}} - T_1\right) L sin\left(\frac{(N_{rotor}-2)}{2N_{rotor}}\pi\right) \\ -W_{total}(sin\theta)CG_R = 0$$

The drag force in Eq. (8) is modeled as a function of the flight speed V_F and the θ_{pitch} based on the results of the wind tunnel test using 'Matrice-100' by KARI.

3.3. Structure analysis module

Based on the 1-D Euler-Bernoulli beam theory, the Structure module checks whether the support rod can tolerate the structural load generated by rotor thrust applied at the tip of the support rod.

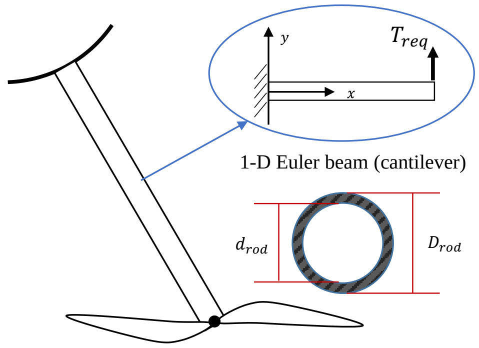

Figure 15: Structure analysis

The stress acting on the rod is calculated by following equations.

(12) $$\sigma_{max} = \frac{g_f T_{req} L (D_{rod}/2)}{I_{zz}} \quad [\text{Pa}]$$

(13) $$I_{zz} = \frac{\pi}{64}\left(D_{rod}^4 - d_{rod}^4\right) \quad [\text{mm}^4]$$

(14) $$\sigma_{allow} = \sigma_{ult}/n_{safe} \quad [\text{Pa}]$$

This study uses 2.0 for the acceleration factor g_f in Eq. (12) and for the safety factor n_{safe} in Eq. (14). When the maximum stress σ_{max} is smaller than the allowable stress σ_{allow}, the support rod withstand the load. This module correlated well with the web-based calculator+) for a 10kg quadrotor equipped with 22 in rotors and 20mm × 18mm × 350mm carbon support rods.

3.4. Aerodynamics analysis module

In the Aerodynamics analysis module, the rotor RPM and the mechanical power P_{mech} are calculated when the required thrust T_{req} is generated at the rotor. Using Blade Element Momentum Theory (BEMT)[10, 11], the calculation was conducted. In calculation, it is assumed that the rotors rotate in an isolated condition without any aerodynamic interference from the adjacent rotors. The equations are following.

+) Advanced Mechanical Engineering Solution (AMES) beamcalculator, accessed at 13/5/2018.
URL: http://www.amesweb.info/StructuralBeamDeflection/CantileverBeamConcentratedLOad.aspx

$$dC_{T,BET} = \frac{1}{2}\sigma C_l r^2 dr,\ dC_{T,MT} = 4\lambda(\lambda - \lambda_c) r dr \tag{15}$$

$$C_T = \int_{r_{root}}^{B} dC_T dr \tag{16}$$

$$\begin{aligned} C_P &= \int_{r_{root}}^{B} dC_{P_i} + \int_{r_{root}}^{1} dC_{P_0} \\ &= \int_{r_{root}}^{B} \kappa dC_T + \int_{r_{root}}^{1} \frac{1}{2}\sigma C_d r^3 dr \end{aligned} \tag{17}$$

In Eq. (16), and (17), the tip loss factor B and the induced power factor κ is 0.88 and 1.25, respectively. This values are derived from the comparison with thrust test results of ‘KPROP’ propeller developed by KARI. Based on the test results, the module is also validated. Figure 16 shows the configurations of ‘KPROP’ and the aerodynamic performance curves of 2 cases. The left column is the configuration curves: chord length distribution (left top) and twist angle distribution (left bottom). Two figures in the top right are comparison curves of Case 1 which uses ‘ClarkY’ airfoil. Case 2 using ‘SG6043’ airfoil is shown in the bottom right. The aerodynamic coefficients of the airfoils are obtained from Xfoil tool[12].

In the comparison of four figures (center and right column), the maximum error is about 4%, indicating the module is reliable at the conceptual design phase.

3.5. EPS analysis module

The last module, EPS analysis, calculates the motor‘s electric power P_{elec}, current I_m, and efficiency η_m to rotate the motor. The schematics of EPS is shown in Figure 17 followed by the equations.

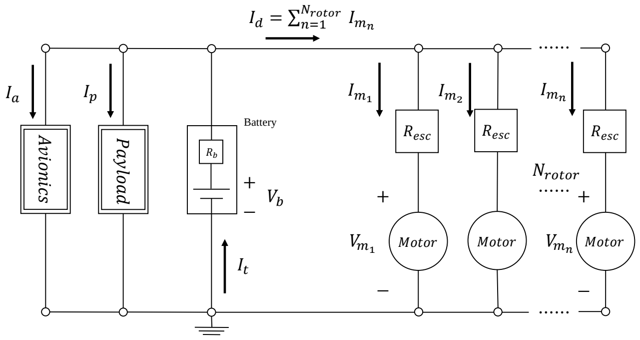

Figure 17: Schematics of EPS

$$I_t = I_d + I_a + I_p \tag{18}$$

$$I_d = \Sigma_{n=1}^{N_{rotor}} I_{m_n} \tag{19}$$

$$V_{m_n} = V_b - (I_d + I_a + I_p)R_b - I_{m_n}R_{esc} \tag{20}$$

$$V_{m_{avg}} = D_t V_b - (I_d + I_a + I_p)R_b - I_{m_{avg}}R_{esc} \tag{21}$$

Total current I_t discharged from the battery is the sum of currents for driving parts I_d, avionics I_a, and payload I_p. The drive current I_d is the sum of all motor currents. The voltage applied to one motor is calculated by Eq. (20), and the averaged motor voltage is presented in Eq. (21). The D_t in Eq. (21) is the throttle signal from ESC which changes supplied battery voltage to control motor RPM. The present study defines the throttle as Eq. (22), indicating pseudo linearity. It means that the RPM of motors is controlled almost linearly with the throttle signal.

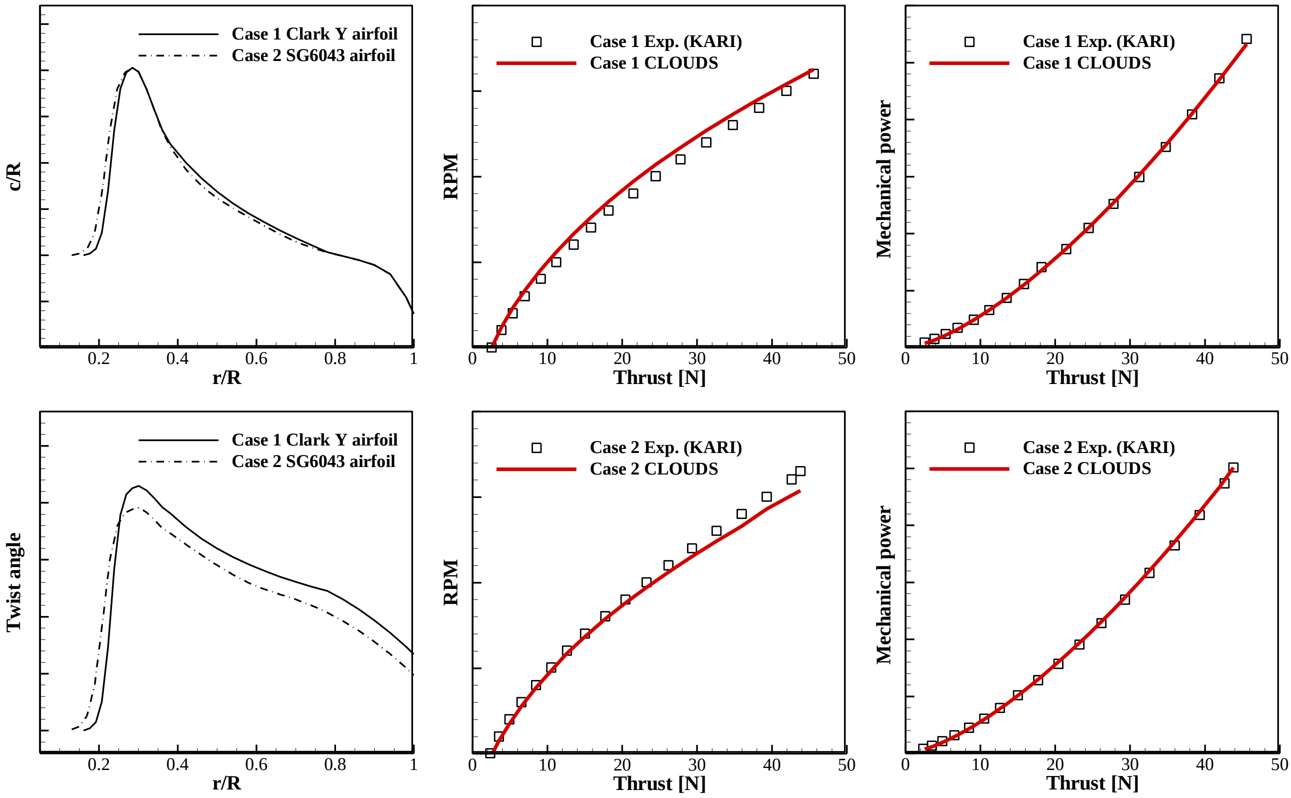

Figure 16: Rotor configuration (Left), Thrust - RPM curve (Center), Thrust - Mechanical power curve (Right)

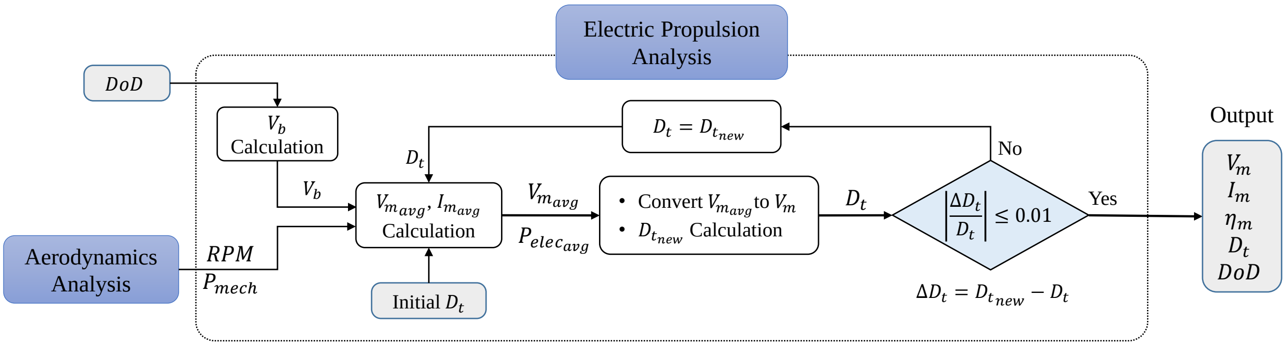

Figure 18: Analysis flowchart of electric propulsion system

(22) $$D_t = \frac{RPM}{RPM_{max}}$$

(23) $$RPM_{max} = V_{emf}K_v = (V_m - I_mR_m)K_v$$

The numerator of the D_t comes from the aerodynamics module and the denominator is obtained by Eq. (23).

When a BLDC motor operates, some losses occur in the motor. They are classified into four categories: Copper loss P_{Co}, Iron loss P_{Ir}, Mechanical loss P_{Me}, and Stray loss P_{St}. In the present study, BLDC motors are modeled with some assumptions[13] (Figure 19).

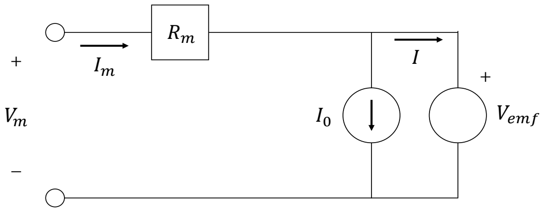

Figure 19: BLDC motor

(24) $$P_{Co} = I_m^2R_m$$ (25) $$P_{Ir} = V_{emf}I_0$$

The two equations above are for the P_{Co} and the P_{Ir}. The R_m and the I_0 can be obtained from the estimation equations in 3.1.2. The P_{Me} and the P_{St} are considered proportional to the P_{mech}[14]. Considering the losses, the power equation is derived as Eq. (26).

(26) $$P_{mech} = P_{elec} - (P_{Co} + P_{Ir} + P_{Me} + P_{St})$$

(27) $$P_{elec} = V_mI_m = V_{m_{avg}}I_{m_{avg}}$$

The calculation algorithm for EPS is presented in Figure 18. Firstly, using the DoD from the previous mission segment, the battery voltage is calculated. Then, the iterative calculation loop starts with the RPM and the P_{mech} coming from the aerodynamics module. Using an initial throttle value, the averaged values such as $V_{m_{avg}}$ and $I_{m_{avg}}$ are calculated by solving the nonlinear simultaneous equations comprised of Eq. (20) ~ (26). After converting the averaged values to instantaneous values by Eq. (27), a new throttle signal is calculated through Eq. (22), and Eq. (23). By comparing the two throttle signal values, the iterative loop terminates when 1% discrepancy occurs between them. As the results of the analysis, the V_m, the I_m, the η_m and the DoD are obtained.

To validate the EPS analysis module, the calculation results are collated with those obtained from the eCalc. Because the eCalc is the experiment-based calculator, it is selected as the reference. To negate the difference of the aerodynamic analysis, the same RPM and P_{mech} values are used. The validation cases and results are shown in Table 1 and Figure 20, respectively. The averaged error rate is 5.5% in throttle, and 3% in the others: P_{elec}, η_m, and hovering time.

Table 1: Validation cases of EPS analysis

Spec.	Case 1	Case 2	Case 3
D_{rotor} [in]	9	22	22
Model	APC		
K_v	920	225	170
Model	DJI 2212-920	Dualsky 5330C-225	T-Motor P60-170
Capacity [Ah]	5	10	6
Cell	4	6	10
A_{max} [A]	50		
Model	Suppo 50A		

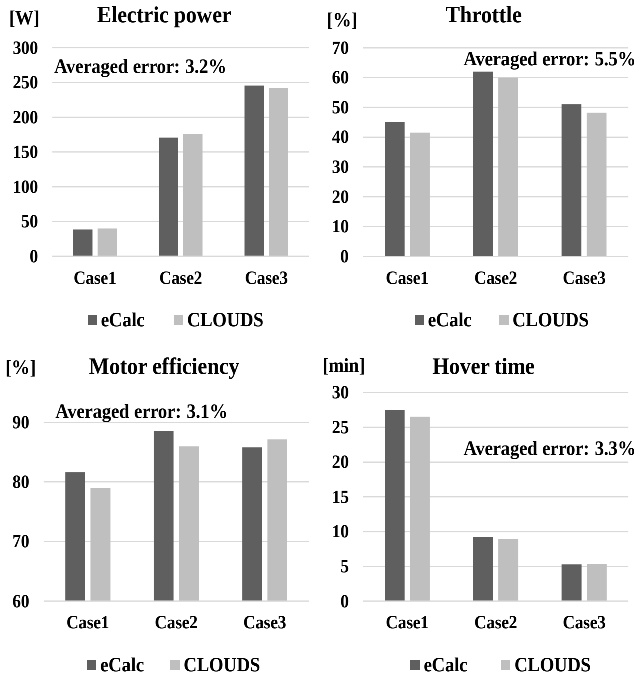

Figure 20: Validation of EPS analysis module

4. THE VALIDATION OF CLOUDS ANALYSIS

Although the verifications and validations of each analysis module were conducted at the module level, it is essential to show the credibility of the framework at the system level. To this end, the hovering times calculated by the CLOUDS are compared with those measured in flight test for four vehicles. The specification of the vehicles and the comparison results are listed at the end of this paragraph (Table 2, 3). The flight test data and the result of the EMST for three models are referred from Ref. [3]. In addition to three referred models, fourth flight test data is obtained from KARI. KARI conducted the flight test with the 'DevKopter'. To calculate flight time in the CLOUDS, all presented methods and models are applied except for the layout of the frame. When using the linear blade model, eight parameters except for D_{rotor} and θ_{tip} are taken from the T-Motor's product. The equations presented in Chapter 3.1 estimates the characteristic values of the motors and the ESCs. The total weight W_{total} is the given input value for calculation.

Table 2: Validation cases of CLOUDS analysis

Spec.	Model 1	Model 2	Model 3	DevKopter
D_{rotor} [in]	28	17	18	18
Pitch [in]	9.2	5.5	5.5	6.1
Model	T-Motor	Foxtech	Foxtech	T-Motor
K_v	100	360	390	420
Model	T-Motor U8	RC timer	Turnigy multi-star	T-Motor U7
Capacity [Ah]	24	13.6	24	16
Cell	6	4	4	6
Model	GEB	Panasonic	GEB	Volt-on
A_{max} [A]	30	20	12	60
Model	Hobby wing	Hobby wing	Turnigy	·
W_{total} [kg]	4.05	1.5	2.1	5.7

Table 3: Comparison of the hovering time [min]

Tested vehicle	Flight test	CLOUDS	Error (%)	EMST
Model 1	129.2	116.9	-9.5	102.5
Model 2	87	88.4	1.6	73.5
Model 3	109.7	108.1	-1.5	107.5
DevKopter	32.3	33.7	4.3	·

Mean absolute error: 4.23

As seen in Table 3, the CLOUDS estimates the hovering time more accurately than the EMST does. This is mainly due to the fact that the multi-disciplinary analysis enables the CLOUDS to calculate the motor efficiency according to the drive components. A more accurate value was obtained, though, the discrepancy between the tests and the CLOUDS' results still exists. This discrepancy may be due to some factors as follows. In the EPS analysis, the implemented model for the BLDC motors is a simplified model, so that the differences to the real products' characteristics may have an error. Secondly, the current drawn by the avionics is a constant value in all flight status in the CLOUDS. In the aerodynamic analysis, the linear blade may also make some discrepancy when estimating the P_{mech}. Furthermore, the influence of the draft and the aerodynamics interference between adjacent rotors are not taken into account for this study. Despite these limits, the CLOUDS has high accuracy at the conceptual design phase, showing low mean absolute error rate, 4.23%.

4.1. Correlations and sensitivity analysis

In conceptual design, it is important to examine the correlations between variables or the influence of each variable on each output of calculation. In order to comprehensively identify the correlations of variables and outputs, the analysis by Self-Organizing Map (SOM) was conducted. SOM is an unsupervised neural network technique that classifies and visualizes the correlation using clustered coloured pattern[15]. The contrary coloured patterns in SOMs mean that two variables are in trade-off relation. Figure 21 shows the results of SOM classified into 15 clusters; red being high value and blue being low value. The inputs are in the left three columns and outputs in the right three columns. Some legacy knowledge is confirmed by the results of SOM. Two patterns of (c)K_v and (d)D_{rotor} show the opposite pattern. Low K_v motors have relatively thinner wire with more wind, meaning high current per a volt. Thus, low K_v motors can generate high torque, and are coupled with large rotors. Additionally, the two SOMs is similar to that of (j)W_{total}. Clusters with heavy W_{total} usually have large D_{rotor} and low K_v (4, 8, 11, 12 clusters). In contrast, clusters with light W_{total} tend to have small D_{rotor} and high K_v (1, 2, 6, 5 clusters). This shows that there is a direct correlation between W_{total} and D_{rotor}, and an inverse correlation between W_{total} and K_v. Furthermore, focusing on the 9th, 12th cluster, it is recognized that the colour changes more in (c)K_v than (d)D_{rotor} when W_{total} gets heavier. From this fact, it is inferred that K_v is more related to W_{total} than D_{rotor} is. Clusters with large capacity have longer flight time, and clusters with small capacity have shorter flight time, showing similar coloured patterns. In contrast, (d)D_{rotor} and (k)RPM show the opposite pattern, indicating an inverse correlation. When comparing the 3rd and the 10th

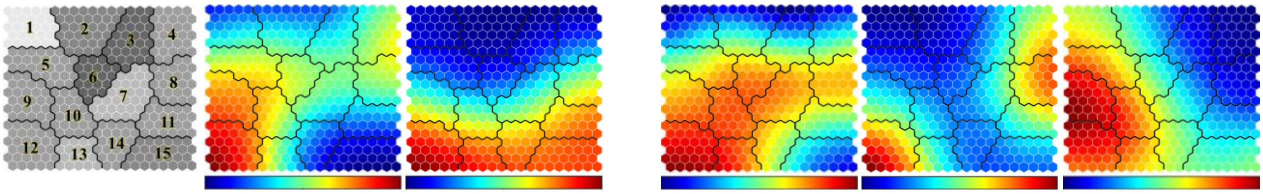

Clustering (a) Capacity (b) Cell (i) Flight time (j) W_{total} (k) RPM

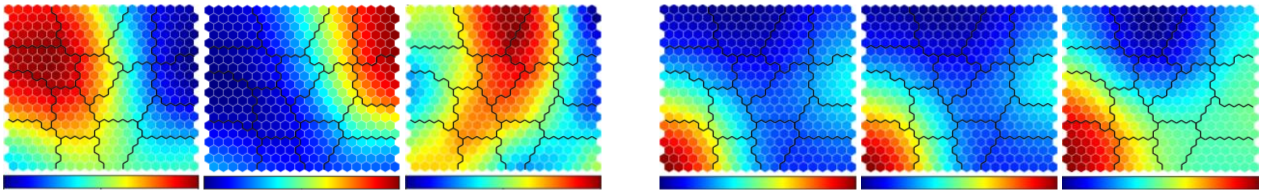

(c) K_v (d) D_{rotor} (e) Pitch (l) P_{mech} (m) P_{elec} (n) η_m

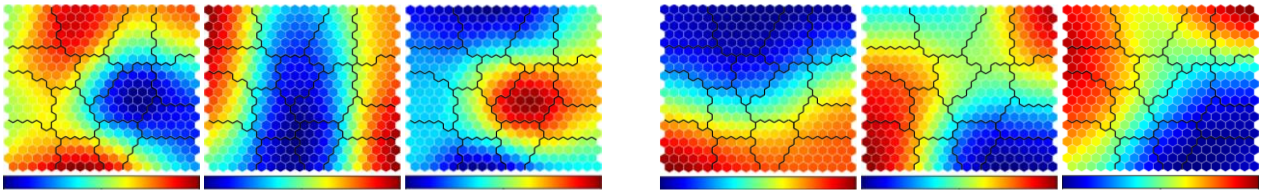

(f) A_{max} (g) L (h) D_{rod} (o) V_m (p) I_m (q) D_t

Figure 21: Results of Self-Organizing Map

clusters having comparable W_{total}, the 3rd cluster with large D_{rotor} has low RPM than the 10th cluster, which affects the (l)P_{mech}. The results of SOM for (j)W_{total} and (l)P_{mech} appear similar pattern except for the vicinity of the 8th cluster. Once again, in clusters 3 and 10, the W_{total} of the two clusters are similar. However, the P_{mech} is smaller in cluster 3 because of the low RPM than in cluster 10.

Through the SOM, it is possible to figure out the relations between variables qualitatively. However, the exact numbers in clusters of SOM have no meaning, so that we could not find quantitative information by SOM. This is the reason why the Analysis of Variance (ANOVA) was performed. To perform ANOVA, the surrogate model was constructed based on Radial Basis Function (RBF). The goodness of fits between estimation and calculation is evaluated by cross-validation analysis, and its results lie in the Appendix. Using the surrogate model, ANOVA was conducted for five outputs of calculation with eight variables that determine the components of UAVs. The results are displayed on the left of Figure 22. The four most influential variables are the K_v, the battery capacity, the number of cell, and the D_{rotor}. The influences of these variables accounted for at least 83% in flight time and up to 91% in W_{total}. The K_v, the battery capacity, the number of cells, and the D_{rotor} are dominant in order for (a)W_{total}. The more significant impact of the K_v than the D_{rotor} is consistent result with the SOM analysis. In (b)P_{mech}, the impact of the D_{rotor} is bigger than that in the W_{total} because of the RPM difference by the D_{rotor}. The D_{rotor} and the number of cells are ranked at the first and the third in (c)P_{elec}. That is because the η_m has effect on the P_{elec}.

The η_m is determined by the combination of the rotor, motor and battery. The result of ANOVA for (d)η_m also shows that the three variables which have a large impact on η_m are the D_{rotor}, the K_v, and the number of battery cells. Since the P_{elec} is eventually calculated normalized by the η_m, this result is obtained; D_{rotor}, K_v, the number of cell are the top three. At last, as mentioned in SOM, the flight time and the battery capacity is highly correlated. Thus, the battery capacity takes third place for (e)Flight time. As a result, we realized that designing the EPS composed with the rotors, the motors and the battery is the most essential part when designing multirotors.

The right line graph in Figure 22 shows the sensitivity of the performance values for the four most prominent variables. The dashed line indicates the specification of DJI Inspire 2. The notable point is that the graphs of the P_{elec}, the η_m, and the flight time exhibit a nonlinear curve as the D_{rotor} and the K_v changes. They all have a local extremum point about the D_{rotor} and the K_v. In perspective of the aerodynamics, the larger the D_{rotor} is, the smaller the P_{mech} gets, resulting in the extension of the flight time. The P_{mech} is continually decreases in the graph. However, the large rotor requires greater torque to rotate. The required torque is directly proportional to the I_m and a torque constant K_t (Eq. 28).

$$(28) \qquad Torque = K_t(I_m - I_0)\ ,\quad K_t = 1/K_v$$

When the small rotor is replaced with a larger one for the same motor, the I_m should be increased to generate torque, which means an increase of the P_{elec}. Therefore, the η_m falls as the D_{rotor} becomes bigger, resulting in the decrease of the flight time. The plotted

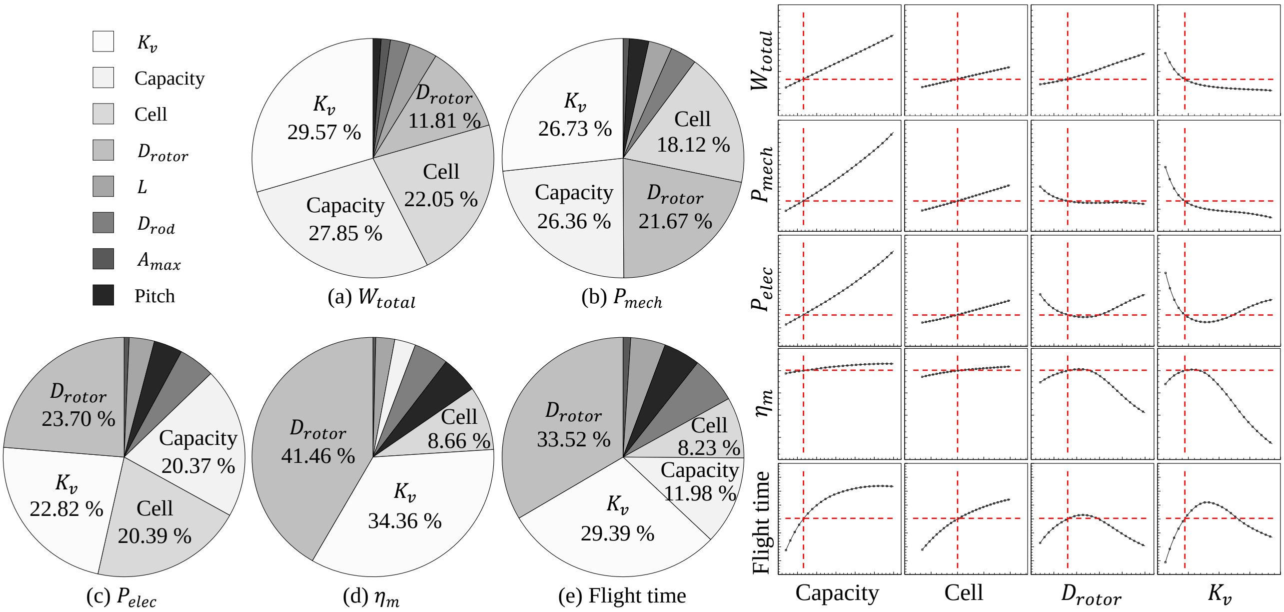

Figure 22: The results of ANOVA & Sensistivities of outputs to variables

graph also supports this fact by showing that the P_{elec}, the η_m, and the flight time charts are bent at almost the same point. Likewise, when substituting high K_v small motors for low K_v big motors, the η_m and the flight time plummet sharply after a certain point. The reason is identical to the rotor case; When high K_v motors are paired with the big rotors, the I_m should surge to generate large torque, then the flight time gets shorter. As described above, it is clear that the performance improvement by a single disciplinary is limited. Thus, the multi-disciplinary analysis that consider the rotor and the motor simultaneously is indispensable to the design of a multirotor UAV.

5. DESIGN OPTIMIZATION

Utilizing the developed framework, the design optimization was conducted. Three configurations according to the number of rotors were designed and their performances were analyzed. The eight variables, which determine the overall size and performance of a multirotor, are designated as the design variables. The optimized solutions are obtained by the Genetic Algorithm. The design space is shown in the Appendix. For a realistic and efficient design process, some assumptions below are used.

1) Material for the rotors and the frame is carbon fiber.
2) Linear blade model is applied with values of APC's product.
3) The P_{Me} and the P_{St} is 1% and 0.5% of the P_{mech} respectively[14].
4) The parameters of the battery are listed below.
   - Allowable C-rate: 65C, Maximum DoD: 85%
5) To ignore aerodynamic interference of rotors, $l_{tip} \geq 0.5$ condition is satisfied[16].
6) The weight of avionics and the I_a is set as 0.05kg, and 0.5A, respectively[3].

5.1. Hovering mission

With the two missions depending on the hovering time, the design optimization was conducted to minimize the W_{total}. The optimization problem and the results are presented below.

- Objective: Minimize W_{total} with the 2kg payload
- Constraint: $D_t \geq 60\%$ at hover

Table 4: The optimization results for hovering mission

Mission	Design variables & W_{total}		The number of rotors		
			4	6	8
Case 1 Hover 15 min. @ 30m altitude with 2kg payload	D_{rotor} Pitch	[in] [in]	10 0	10 1	9 2
	K_v		859	965	1250
	Capacity Cell	[Ah]	11.097 5	12.211 4	16.584 3
	A_{max}	[A]	23	22	21
	D_{rod} L	[mm]	10 142	10 236	10 300
	W_{total}	[kg]	4.601	4.735	4.851
	Diagonal length	[mm]	449	637	749
Case 2 Hover 30 min. @ 30m altitude with 2kg payload	D_{rotor} Pitch	[in] [in]	20 1	16 1	15 1
	K_v		239	445	542
	Capacity Cell	[Ah]	34.468 6	37.675 5	42.080 4
	A_{max}	[A]	44	35	28
	D_{rod} L	[mm]	12 284	12 376	10 500
	W_{total}	[kg]	11.315	10.324	9.918
	Diagonal length	[mm]	898	1016	1248

All six designed vehicles are constructed with the optimal combination of the rotors, the motors, and the number of battery cells. As the number of rotors increases, the D_{rotor} gets smaller because thrust per rotor decreases. The battery paired with high K_v motors has fewer cells. These results come from applying the D_t through the multi-disciplinary analysis. Eq. (22) for the D_t is comprised of the rotor RPM and the EPS analysis. Thus, for an adequate D_t value at flight, the D_{rotor}, the K_v, and the number of cells should be matched with one another. The weight fraction and the maximum performance values of the six designed multirotors are shown in Figure 23. The Left bar chart shows the weight fraction of the components weight. In case 1 with shorter hovering time, the quadrotor is the most lightweight layout. When the rotors are added, the total weight of motors and ESCs and their fraction rise despite the lighter single part. The frame weight and its fraction also increases as the number of rotors increases. The performance of the designed multirotors is different to one another. The quadrotor has the smallest maximum vertical rate of climb (VROC), because it has the zero pitch value. The low pitch means a small twist angle of the rotor blade. When moving upward, the effective angle of attack of rotor blades is reduced by the inflow from the VROC, requiring higher RPM to generate thrust. Therefore, the rotor with low pitch reaches its maximum RPM earlier, implying relatively low VROC. The hexarotor and octarotor with higher pitch could climb faster than the quadrotor. As the vehicle has more rotors, the maximum V_F declines. That is because the drag force acting on the vehicle inclines due to its expanded dimension. In addition, since the size of the motors gets smaller, the P_{max} of the motor also gets smaller, reaching the limit earlier. Hence, the quadrotor has the fastest cruise ability. The hexarotor has the heaviest payload capability. When more rotors are used, the weight per rotor is reduced, so that the payload weight could be enlarged. Nevertheless, the hexarotor can lift heavier payload than the octarotor does. This is because a smaller rotor is equipped to the octarotor. Accordingly, the increment of the RPM is high, which rapidly reaches the RPM limit when lifting the payload. In contrast to the case 1, for the case 2 with longer hover mission, the octarotor is the most lightweight configuration. On the other hand, the quadrotor is the heaviest. Although the quadrotor has fewer rotors, the total weight of motors of it is the heaviest. This is because the single motor weight increases exponentially as the K_v become smaller. Due to the big rotors and the motors, the battery requires more cells to maintain an adequate D_t. Furthermore, the center plate of the body frame is dependant on the D_{rotor}, so that the frame of the quadrotor is heavy. In the hexa and octarotor, despite their many rotors, the total weight of motors is smaller than quadrotor's due to the high K_v. The fewer battery cells contribute to the reduction of the battery weight. For these reasons, the quadrotor is the heaviest layout for longer hover mission. The performance of the three UAVs shows similar trend to the presented case 1. The maximum V_F declines owing to the increasing drag, and the hexarotor can lift the heaviest payload.

6. CONCLUSION

The integrated design optimization framework is developed with brand-new analysis algorithm of the EPS for the electric driven multirotor UAVs. This framework shows the improved accuracy in estimating the flight time than another tool due to the multi-disciplinary analysis. For efficient design procedure, the modeling methods of each component are also suggested. The correlations between variables and their impact on the performance are found by SOM,

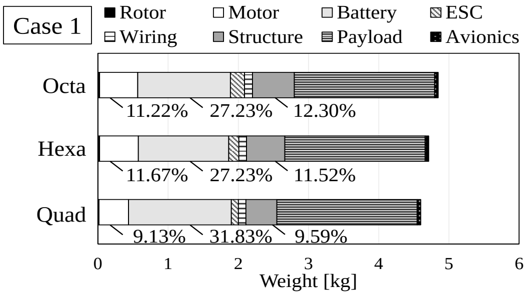

Unit: [kg]	Quad	Hexa	Octa
Rotors	0.016	0.024	0.024
Motors	0.420	0.552	0.544
Battery	1.464	1.288	1.320
ESCs	0.100	0.144	0.200
Wiring	0.108	0.109	0.113
Structure	0.441	0.545	0.596
Payload	2.000	2.000	2.000
Avionics	0.050	0.050	0.050

Performance	Quad	Hexa	Octa
Max. VROC [m/s]	15.0	16.0	16.0
Max. V_F [m/s]	31.8	28.8	27.2
Max. Hover time [min]	34.00	32.92	32.38
Max. Payload [kg]	3.3	4.6	3.7

VROC: Vertical Rate of Climb

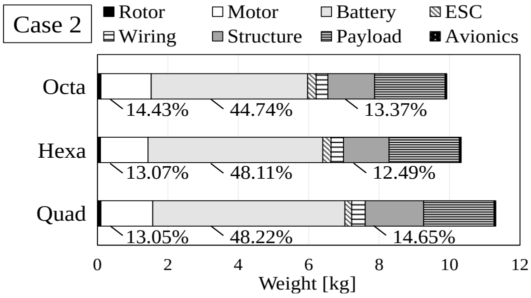

Unit: [kg]	Quad	Hexa	Octa
Rotors	0.096	0.084	0.096
Motors	1.476	1.350	1.432
Battery	5.455	4.969	4.440
ESCs	0.196	0.234	0.248
Wiring	0.383	0.352	0.330
Structure	1.657	1.290	1.327
Payload	2.000	2.000	2.000
Avionics	0.050	0.050	0.050

Performance	Quad	Hexa	Octa
Max. VROC [m/s]	18.0	19.0	17.0
Max. V_F [m/s]	32.4	30.2	25.3
Max. Hover time [min]	40.03	41.37	42.00
Max. Payload [kg]	7.1	8.1	7.9

Figure 23: Weight fration & performance of the designed multirotor

ANOVA, and sensitivity analysis. Through this, it is confirmed that the multi-disciplinary analysis is essential to design multirotors due to their non-linearity of the performance variance. Utilizing the framework, the design optimization was conducted for the two missions with different hovering time. Through the optimizations, it was found that the quadrotor is suitable to the shorter mission, and the octarotor is desirable for the more extended mission.

ACKNOWLEDGEMENT

This research was supported by Unmanned Vehicles Advanced Core Technology Research and Development Program through the National Research Foundation of Korea (NRF), Unmanned Vehicle Advanced Research Center (UVARC) funded by the Ministry of Science and ICT, the Republic of Korea (NRF-2016M1B3A1A03937680).

REFERENCES

[1] Cai, G., Dias, J. and Seneviratne, L., “A survey of small-scale unmanned aerial vehicles: Recent advances and future development trends,” *Unmanned Systems*, Vol.2, No.2, 2014, pp.175-199.

[2] Kumar, V., and Michael, N., “Opportunities and challenges with autonomous micro aerial vehicles,” *The International Journal of Robotics Research,* Vol.31, No.11, 2012, pp.1279-1291.

[3] Bershadsky, D., Haviland, S., and Johnson E.N., “Electric multirotor propulsion system sizing for performance prediction and design optimization,” AIAA SciTech 2016, AIAA, San Deigo, CA, Jan. 2016.

[4] Winslow, J., Hrishikeshavan, V., and Chopra, I., “Design methodology for small scale unmanned quadrotors,” 55th AIAA Aerospace Sciences Meeting, Grapevine, TX, Jan. 2017.

[5] Gur, O., and Rosen, A., “Optimizing electric propulsion systems for unmanned aerial vehicles,” *Journal of Aircraft,* Vol.46, No.4, Jul. 2009.

[6] Kraft, D., “A Software Package for Sequential Quadratic Programming,” Tech. Rep. DFVLR-FB 88-28, DLR German Aerospace Center – Institute for Flight Mechanics, Köln, Germany, 1988.

[7] Clerc, M., “Standard particle swarm optimisation,” Technical report, Particle Swarm Central, 2011. Available: http://hal.archives-ouvertes.fr/hal-00764996

[8] Deb, K., Pratap, A., Agarwal, S. and Meyarivan, T.A.M.T., “A fast and elitist multiobjective genetic algorithm: NSGA-II,” *IEEE transactions on evolutionary computation*, Vol.6, No.2, 2002, pp.182-197.

[9] Johnson, W., “NDARC-NASA design and analysis of rotorcraft, validation and demonstration,” AHS Aeromechanics Specialists’ Conference, San Francisco, CA, Jan. 2010.

[10] Leishman, J.G., “Principles of Helicopter Aerodynamics,” 2nd edition, Cambridge Aerospace Series, Cambridge University Press, NY, 2006.

[11] Johnson, W., “Helicopter Theory,” 1st edition, Princeton University Press, Princeton, NJ, 1980.

[12] Drela, M., “XFOIL: an analysis and design system for low Reynolds number airfoils,” *Low Reynolds Number Airfoil Aerodynamics*, edited by T.J. Mueller, Vol.54, Lecture Notes in Engineering, Springer-Verlag, Berlin/New York/Heidelberg, Jun. 1989.

[13] Lawrence, D., and Mohseni, K., “Efficiency analysis for long-duration electric MAVs,” AIAA Infotech@ Aerospace, Arlington, VA, Sep. 2005.

[14] Ilka, R., Tilaki, A.R., Alamdari, H.A., and Baghipour, R., “Design optimization of permanent magnet-brushless DC motor using Elitist genetic algorithm with minimum loss and maximum power density,” *International Journal of Mechatronics, Electrical and Computer Technology,* Vol.4, No.10, 2014, pp.1169-1185.

[15] Jeong, S., Chiba, K. and Obayashi, S., “Data mining for aerodynamic design space,” *Journal of aerospace computing, information, and communication*, Vol.2, No.11, 2005, pp.452-469.

[16] Tanabe, Y., Aoyama, T., Masahiko, S., Hideaki, S., Shigeru, S., Koichi, Y., Hiroshi, T., “Numerical simulations of aerodynamic interactions between multiple rotors,” 42nd European Rotorcraft Forum, Lille, France, Sep. 2016.

APPENDIX

A1. Cross-validation results

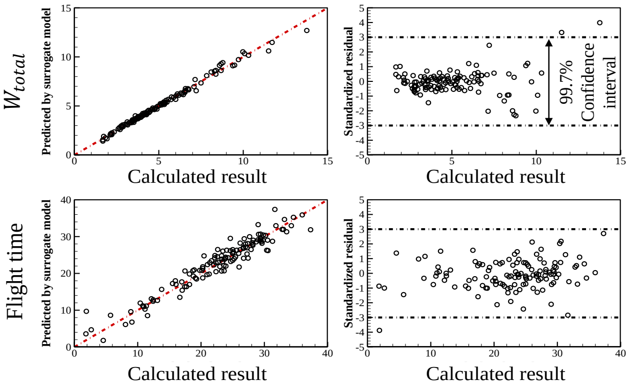

A2. Design space

Design variables		Design space
Rotor	D_{rotor} [in]	$4 \leq D_{rotor} \leq 30$
	Pitch [in]	$0 \leq Pitch \leq 10$
Motor	K_v	$100 \leq K_v \leq 1500$
Battery	Capacity [Ah]	$2 \leq Capacity \leq 50$
	Cell	$2 \leq Cell \leq 12$
ESC	A_{max} [A]	$10 \leq A_{max} \leq 80$
Structure	D_{rod} [mm]	$10 \leq D_{rod} \leq 30$
	L [mm]	$100 \leq L \leq 800$
